PHYSICAL REVIEW A VOLUME 22, NUMBER 5 NOVEMBER 1980

Benchmark cross sections for electron-impact excitation of $n\ ^1S$ levels of He

B. Van Zyl,* G. H. Dunn,† G. Chamberlain,† and D. W. O. Heddle‡
Joint Institute for Laboratory Astrophysics, National Bureau of Standards and University of Colorado, Boulder, Colorado 80309
(Received 9 May 1980)

Absolute total emission cross sections have been measured for electron-impact excitation of He giving radiation from the $6\ ^1S$-$2\ ^1P$, $5\ ^1S$-$2\ ^1P$, $4\ ^1S$-$2\ ^1P$, and $3\ ^1S$-$2\ ^1P$ transitions. Electron energies were 50, 100, 500, 1000, and 2000 eV. Particular care was taken to make the measurements accurate and to make knowledgeable assessments of uncertainties, so that the results serve as reliable benchmarks for calibration of other excitation apparatus as well as for comparison with theory. The most accurate results are for 500-eV electron energy, where the mean uncertainty is only 3.5% high confidence level. The measured emission cross sections are modified to account for branching and cascade to give level-excitation cross sections, and results are compared with other experimental data and theoretical predictions. At 2000 eV, the measurements average 2.5% below Born-approximation calculations.

I. INTRODUCTION

Over the past half century, there have been over 200 papers published dealing with experimental study of electron-impact excitation of He atoms, and at least 100 of these have been written within the past decade. Bibliographies on this voluminous work and the work on other species have been compiled[1-3] and a data compilation published.[4] There are also a number of reviews covering samples of the data and the methods and problems involved in obtaining the results.[5-7] Basic motivations for learning about electron-impact excitation of various species range from the desire to understand nature's processes, to the need to know such cross sections in order to interpret atmospheric and astronomical phenomena; and to apply such data to design problems in illumination, rocket engines, controlled thermonuclear fusion reactors, and other plasma devices. The reader will surely be impressed by the apparent superfluity of adding yet another paper to this seeming glut of information. Indeed, these authors are so impressed, and thus feel compelled to describe fully the motivation and goals of the present work.

Helium is probably the simplest and most straightforward subject for experimental investigation. Yet, a study of the impressive volume of research papers available reveals gross inconsistencies among results by different investigators and the lack of objective criteria for choosing from among these results. This is emphasized by Fig. 1 which shows a sample of the measured cross sections as a function of electron energy for emission of He spectral lines involving $n\ ^1S$-$2\ ^1P$ transitions. These cross sections as a class should be relatively free from subtle experimental problems involving radiation polarization, radiation trapping, excitation transfer, and other difficulties recognized[5] as leading to error in excitation measurements. Yet, as seen, there are substantial disagreements within the data presented, all from "modern" experiments. Because the subtle problems noted above should not strongly affect these particular measurements, one may conclude that difficulties associated with measurement of the basic parameters in these experiments are major causes of error. That is, the techniques of gas density measurement, electron current measurement, and in particular, absolute radiometry, have inherent problems and difficulties not easily discovered by the experimenter.

It is the purpose of this work to measure the $n\ ^1S$-$2\ ^1P$ emission cross sections with enough accuracy and knowledge of uncertainties that other workers will be able to use these results to calibrate their instruments and to verify the reliability of their own techniques. This requires giving painstaking attention to the basic experimental procedures of absolute radiometry, target density determination, and electron-beam handling and measurement. In this paper attention is thus given to detailing the techniques used, and more than usual consideration is given to assessing possible uncertainties in the measured parameters. In this context our goal here is to provide "benchmarks" for optical excitation experiments.

Particular attention has been given to measurement of the He line emission cross sections at 728.1 nm ($3\ ^1S$-$2\ ^1P$), 504.8 nm ($4\ ^1S$-$2\ ^1P$), 443.8 nm ($5\ ^1S$-$2\ ^1P$), and 416.9 nm ($6\ ^1S$-$2\ ^1P$) for 500-eV electron energy. This energy should be accessible to those undertaking both "high-energy" and "low-energy" investigations. More limited data are presented for 50, 100, 1000, and 2000 eV electron energies. Excitation cross sections are obtained from the measured emission cross sections by accounting for branching and cascade processes, and these results are compared with predictions of the Born approximation at the highest energies.

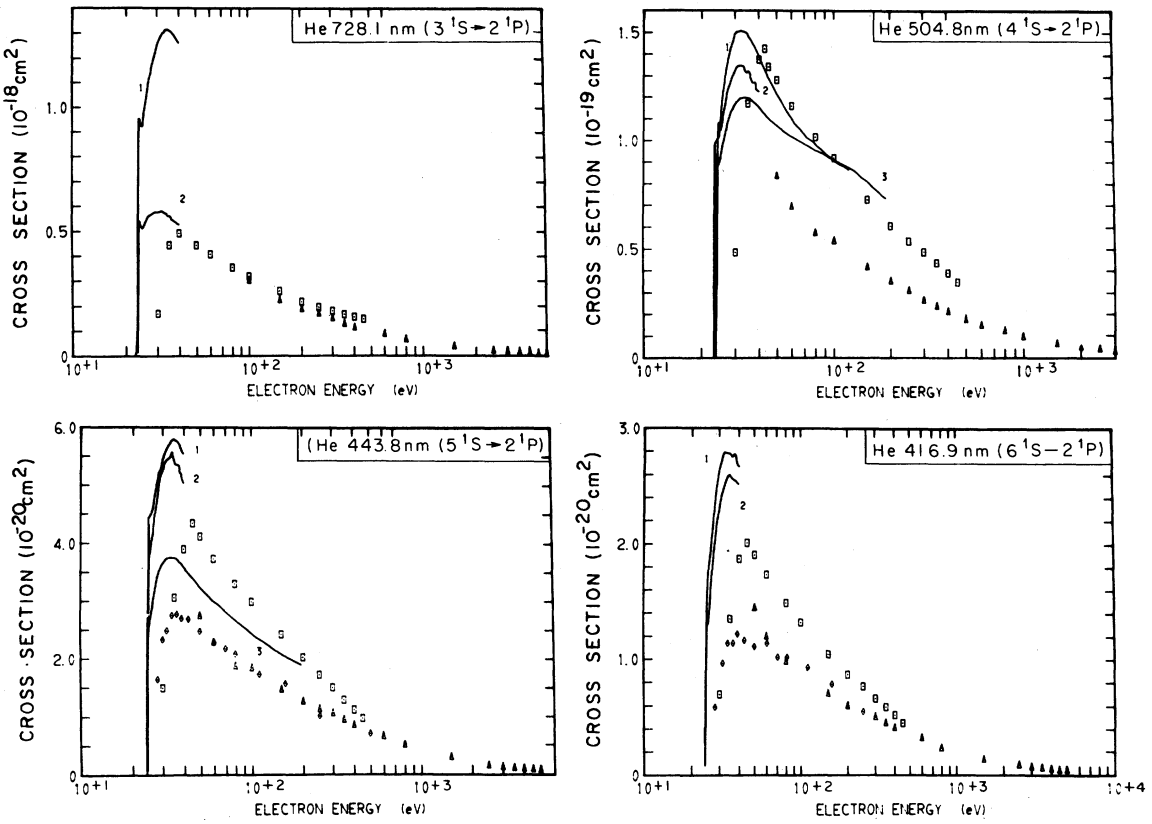

FIG. 1. Experimental line-emission cross sections versus energy for lines and transitions in He as shown in upper right of the figures. 1: Zapesochnyi *et al.* (Ref. 30); 2: Jobe *et al.* (Ref. 35); 3: Yakhontova (Ref. 29); □: Miller (Ref. 36) and St. John *et al.* (Ref. 22); △: Moussa *et al.* (Ref. 16); ◇: Lees (Ref. 28).

Comparisons are also made with other available experimental and theoretical results.

II. GENERAL APPROACH AND THEORY OF THE EXPERIMENT

The experimental configuration follows readily from the specific goals and purposes of this work: An electron gun produces a beam which passes through a collision cell containing He at an accurately measured density, and light produced in e^-+He collisions is measured by a calibrated spectroradiometer. A schematic view of how this was realized is shown in Fig. 2.

The electron gun produces a beam (2 to 200 μA) which traverses the collision cell (typically at about 8×10^{-4} Torr He pressure) and is collected in a deep Faraday cup. Light from a short segment of the beam path (~0.32 mm) at the cell center is collected by an achromat lens and focused onto the entrance slit of a grating monochromator. After passing through the monochromator, the light passes through an interference filter and is focused onto the photocathode of a cooled photomultiplier. Multiplier pulses are counted by two scalers, gated alternately in synchronism with a chopper wheel (50% duty cycle), for signal-dark count separation. For calibration, the entire spectroradiometer can be rotated to view the cavity of a copper-melting-point blackbody or the filament of a tungsten strip lamp.

Define the optical axis of the spectroradiometer entrance lens system to be the z axis, the axis of the electron beam as the x axis, and y as the third orthogonal (vertical) axis. Let θ be the angle a light ray makes with the z axis, and ϕ the angle of the ray about the z axis. The number of photons of wavelength λ_0 emitted from excited He atoms/sec per unit volume/sr can be written as

$$\frac{dn(x,y,z,\lambda_0)}{dV(x,y,z)d\Omega} = \frac{1}{4\pi} N_{\mathrm{He}}(x,y,z)N_e(x,y,z)\sigma(\lambda_0)v_e(x,y,z), \quad (1)$$

where N_{He} and N_e are the He atom and electron densities, respectively, $\sigma(\lambda_0)$ is the line emission cross section, and v_e is the relative velocity of electrons and He atoms. When the spectroradiometer is aligned to collect light from electron-

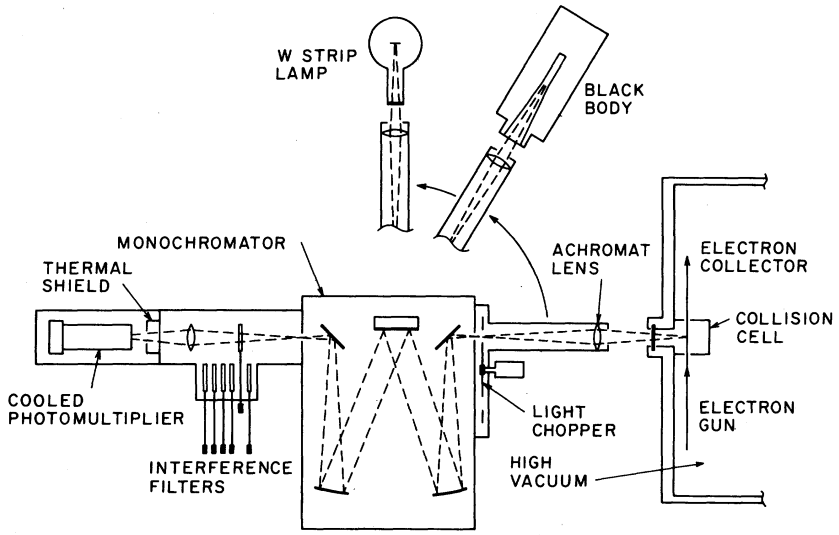

FIG. 2. Schematic view of experimental apparatus. An electron gun operating in high vacuum ($\sim 10^{-7}$ Torr) bombards He gas in a collision cell ($\sim 6\times 10^{-4}$ Torr). Part of the light emitted by excited He atoms enters a spectroradiometer where it is chopped by a mechanical wheel, dispersed successively by grating optics and an interference filter, and counted by a cool photomultiplier and associated electronics. The spectroradiometer can be rotated to view a copper-point blackbody or a W strip lamp, both used as standards for calibration. Not shown in this plane view is an electron-beam-probe–Faraday cup assembly (see Fig. 4).

helium collisions, the photon count rate will be given by

$$R_e=\frac{N_{\mathrm{He}}}{4\pi}\sigma(\lambda_0)\int T_c(x,y,z,\theta,\phi,\lambda_0)T_m(x,y,z,\theta,\phi,\lambda_0)T_f(x,y,z,\theta,\phi,\lambda_0)S(\lambda_0-\lambda_0)\epsilon(x,y,z,\theta,\phi,\lambda_0)\Gamma_e(x,y,z)d\Omega\,dV\,, \tag{2}$$

where N_{He} is taken as independent of position in the cell and the electron flux $\Gamma_e(x,y,z)=N_e(x,y,z)v_e(x,y,z)$. Here T_c is the transmission of the collision cell window, T_m is the transmission of the monochromator and its associated optical components, T_f is the transmission of the interference filter, $S(\lambda-\lambda_0)$ is the monochromator slit function normalized to unity at $\lambda=\lambda_0$, and ϵ is the combined efficiency of the photomultiplier and electronics for registering a pulse.

If $L_s(\lambda)$ is now defined as the radiance of the strip lamp standard source in photons/sec per $\Delta\lambda$ per cm^2 of source area/sr, and T_s as the strip-lamp window transmission, a similar expression (but involving an integration over λ as well) can be written for the photon count rate R_s from this source. Dividing these equations and solving for $\sigma(\lambda_0)$ gives

$$\sigma(\lambda_0)=\left(\frac{4\pi}{N_{\mathrm{He}}}\right)\left(\frac{R_e}{R_s}\right)\frac{\int T_s(x,y,z,\theta,\phi,\lambda)}{\int T_c(x,y,z,\theta,\phi,\lambda_0)}$$
$$\times\frac{T_m(x,y,z,\theta,\phi,\lambda)T_f(x,y,z,\theta,\phi,\lambda)L_s(\lambda)S(\lambda-\lambda_0)\epsilon(x,y,z,\theta,\phi,\lambda)\cos\theta\,d\Omega\,dA\,d\lambda}{T_m(x,y,z,\theta,\phi,\lambda_0)T_f(x,y,z,\theta,\phi,\lambda_0)S(\lambda_0-\lambda_0)\epsilon(x,y,z,\theta,\phi,\lambda_0)\Gamma_e(x,y,z)dV\,d\Omega}\,, \tag{3}$$

where $\cos\theta\,dA$ is the elemental area viewed on the strip lamp.

Define position z_0 along the spectroradiometer optical axis z as that position at which the image of the light source viewed is focused onto the monochromator entrance slit and assume that the strip-lamp filament is situated at $z=z_0$. Furthermore, assume that the diameter of the electron beam in this dimension, $2(\Delta z)$, is sufficiently small that the approximation $z=z_0\pm\Delta z\approx z_0$ can be made to high accuracy, so that z can be replaced by z_0 everywhere in Eq. (3) except in $\Gamma_e(x,y,z)$. If the electron beam is now taken to travel parallel to the x axis over the small Δx observed, $\Gamma_e(x,y,z)$ can be replaced by $\Gamma_e(y,z)$, which can be integrated over its z dependence to give $E(y)$, i.e.,

$$E(y)=\int\Gamma_e(y,z)dz\,, \tag{4}$$

with $E(y)$ satisfying the normalization

$$\int E_e(y)dy = \frac{I_e}{e}\,, \tag{5}$$

where I_e is the total electron current and e the electron charge.

Since the collision cell and strip-lamp windows are high-quality optical components, their transmissions T_c and T_s should be independent of the parameters x, y, z, θ, and ϕ over the small ranges of these variables covered in this experiment. Furthermore, since the variations of T_s, T_m, and ϵ with λ for small $\Delta\lambda$ about λ_0 (i.e., over the spectroradiometer bandpass with the monochromator set at λ_0) should be small, the dependence of these parameters on λ can be ignored. Finally, if it is assumed that the position and wavelength dependences of the interference filter transmission can be separated, i.e.,

$$T_f(x,y,z,\theta,\phi,\lambda) \approx F(\lambda)T_f(x,y,z,\theta,\phi,\lambda_0)\,, \tag{6}$$

where $F(\lambda)$ is the normalized filter transmission profile relative to unity at $\lambda=\lambda_0$, the wavelength integration in the numerator of Eq. (3) can be performed to give

$$\mathcal{L}_s(\lambda_0) = T_s(\lambda_0)\int S(\lambda-\lambda_0)F(\lambda)L_s(\lambda)d\lambda\,, \tag{7}$$

the reduced strip-lamp radiance at λ_0.

The approximations made above will be investigated in Sec. III where the uncertainties associated with their use will be evaluated. Under these assumptions, and taking $\cos\theta \approx 1$ ($\theta \lesssim 3°$ in the experiment), Eq. (3) reduces to

$$\sigma(\lambda_0) = \left(\frac{R_e}{N_{\mathrm{He}} I_e}\right)\left[\frac{4\pi e \mathcal{L}_s(\lambda_0)\mathcal{K}'}{T_c R_s}\right], \tag{8}$$

where $\mathcal{K}'$ is given by

$$\mathcal{K}' = \frac{\int D(y,\lambda_0)dy \int E(y)dy}{\int D(y,\lambda_0)E(y)dy} \tag{9}$$

and $D(y,\lambda_0)$ by

$$D(y,\lambda_0) = \int T_m(x,y,z_0,\theta,\phi,\lambda_0)T_f(x,y,z_0,\theta,\phi,\lambda_0) \times \epsilon(x,y,z_0,\theta,\phi,\lambda_0)d\Omega\,dx\,. \tag{10}$$

Here $D(y,\lambda_0)$ is essentially the sensitivity of the spectroradiometer as a function of the vertical coordinate y. Note that if $D(y,\lambda_0)$ is relatively independent of y over the region where $E(y)$ is finite, $\mathcal{K}'$ is essentially the height of the area viewed on the strip-lamp source.

Implicit in the development of the above equations, has been the assumption that the emission resulting from e-He collisions maps identically to the electron density. This would be true if the excited-state lifetimes were zero. In fact, the lifetimes of the $3\,^1S$, $4\,^1S$, $5\,^1S$, and $6\,^1S$ states are, respectively, 55, 75, 155, and 279 nsec (Ref. 8); so that with a mean velocity of 5.7×10^4 cm/sec (308 K), an excited $6\,^1S$ atom (for example) will travel about 0.16 mm in one lifetime, far enough to require a correction to the above results.

Motion in the x direction will not affect the observed count rate; since for every excited atom that moves from position x' (in the spectroradiometer's viewing field) to position $x'+\delta$ (outside the field) before decaying, there is an atom which moves from $x'-\delta$ to x'. Similarly, motion in the z direction is not important, since (as will be shown in Sec. III) the spectroradiometer sensitivity varies nearly linearly for small displacements about z_0. Thus, one need only consider motion in the y direction.

An atom with velocity v_y and excited-state lifetime τ which is excited at point y' has probability per unit length of decaying at y given by

$$P'(y,y',v_y) = \left(\frac{1}{v_y\tau}\right)e^{-(y-y')/v_y\tau}\,. \tag{11}$$

The He atoms have a Boltzmann distribution of velocities $F(vy)$, so that we have

$$P(y,y') = \int P'(y,y',v_y)F(v_y)dv_y\,. \tag{12}$$

Since there is a distribution of excitation which does map the electron-beam distribution $E(y')$, one can write the distribution of radiating particles

$$I(y) = \int P(y,y')E(y')dy'\,. \tag{13}$$

Thus the $\mathcal{K}'$ in Eq. (8) must be replaced by

$$\mathcal{K} = \frac{\int D(y,\lambda_0)dy \int I(y)dy}{\int D(y,\lambda_0)I(y)dy}\,. \tag{14}$$

Equation (8), together with defining Eqs. (4), (7), (10), and (14), serve to identify the quantities which must be measured in this experiment. These measurements are described in the next section and their uncertainties evaluated. Before proceeding, however, it is useful to discuss the evaluation of uncertainties in general terms.

The evaluation of the uncertainties in these measurements is of comparable importance to the measurements themselves. In all cases where a variable could be directly measured (length, area, time, etc.), enough measurements were made to get a good estimate of the statistical variance and standard deviation of the individual measurements. Where appropriate, mean values were computed, and the uncertainties taken to be about 2.4σ, effectively 98% confidence level (CL) for the data (here σ is the standard deviation of the mean). When a variable could not be determined by procedures

yielding such measurement statistics, careful assessment was made of the possible uncertainties at a conservative enough level that they could be placed on a "par" with the 98% CL of the statistical uncertainties. Since all uncertainties encountered in the determination of any given parameter were judged to be noncorrelated or independent, they were combined in quadrature. This combination of statistical and systematic uncertainties leads us to use the term "high confidence level" (HCL), estimated to be comparable with 98% confidence level associated with the statistical uncertainties. The total uncertainty was obtained by quadrature combination of the uncertainties in the required parameters, but the latter have been tabulated separately so readers can make their own considered combination of uncertainties if they wish.

It was our policy, whenever possible, to measure each parameter entering the cross section determination by more than one technique. In some cases, a given technique was found clearly superior, and this value with its uncertainty was adopted. In other cases, an average from the several techniques was used and the adopted uncertainty is discussed in the text where appropriate. In this experiment we did not measure the polarization of the emitted $n\,^1S$-$2\,^1P$ radiation. The polarization is theoretically zero, and this has been verified by previous workers.[9,10]

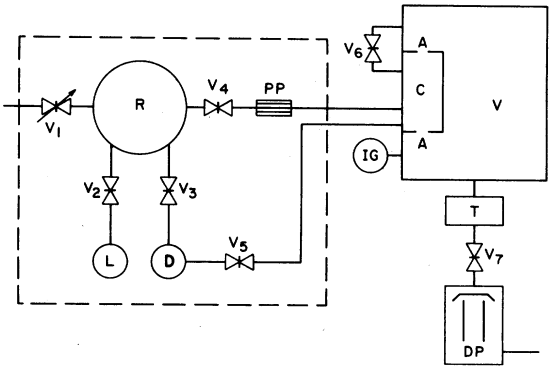

FIG. 3. Schematic of pressure generator. Gas enters standard volume R from a source at the left through leak V_1. Pressure in R is measured either with precision-oil manometer L or capacitance manometer D. Flow continues through V_4 and porous plug PP, into the cell C, out a pair of thin apertures A into high vacuum region V, and finally out through a fast oil-diffusion pump. Dashed lines around R and associated components represent a thermally isolating box. C and V can be heated to measured temperatures with a heating mantle. Not shown are the fore vacuum system with associated bypasses, etc., nor the high vacuum reference for the oil and capacitance manometers.

III. EXPERIMENTAL MEASUREMENTS AND UNCERTAINTY EVALUATIONS

A. Helium density measurements

The target density of He atoms was determined by a dynamic expansion technique which has been described in detail elsewhere.[11] Figure 3 schematically illustrates the procedure used. High-purity He enters the high-pressure reservoir R, through a flow-control valve V_1. This high pressure (0.1 to 1.0 Torr) can be measured by either a precision micrometer-point-contact oil manometer L, used as the local standard, or a calibrated capacitance manometer D. The He exits the reservoir through a porous plug PP, with measured conductance, and enters the low-pressure e^- + He collision cell C. Flow proceeds after many wall collisions through two 2-mm diameter holes A, in the cell wall (also serving as entrance and exit apertures for the e^- beam), and into a fast oil-diffusion pump DP.

The He density in the collision cell is given by

$$N_{He}=9.656\times10^{18}\left(\frac{P_R}{T_R}\right)\left[\left(\frac{F_P}{F_C+F_P(T_C/T_R)^{1/2}}\right)+\left(\frac{P_V}{P_R}\right)\left(\frac{F_C}{F_C+F_P(T_C/T_R)^{1/2}}\right)\right], \tag{15}$$

where P_R is the pressure in Torr in R, T_C and T_R are the temperatures of C and R in K, respectively, F_P is the measured conductance of PP, F_C is the computed combined conductance of apertures A, and P_V is the vacuum tank pressure. Careful analysis and testing showed that density determinations (in the 10^{-3} to 10^{-4} Torr range) with an uncertainty of ±1.2% HCL could be made with this approach. The cross sections reported here at 0.5-, 1.0-, and 2.0-keV electron energy were measured using this technique.

For the 50- and 100-eV cross section data, the pressure in C was measured directly with the calibrated capacitance manometer. Because of the low electron currents available at these energies (see next section), collison-cell pressures of about 2×10^{-3} Torr were required to obtain reasonable photon-counting signals. The estimated HCL uncertainties associated with the density measurements using this latter method were judged to be ±3.0%.[12]

It has already been noted that emissions from the $n\,^1S$ levels of He should be relatively free from such pressure-dependent effects as resonance-radiation trapping and excitation transfer. However, radiation trapping will affect the cascade contributions to the observed emissions from higher $n\,^1P$ levels, and it is possible that secondary electrons

from ionization could produce an effect. Heddle and Samuel[13] have investigated the effect of resonance trapping in the $3\,^1P$ state of He and modeled its magnitude for various collision-cell geometries. However, for a cell such as ours, the parameters entering the evaluation are not easily defined. In view of this and the possible contributions from secondary electron excitation, the apparent emission "cross sections" were measured as a function of cell pressure. For the 728.1-nm line, the apparent cross section increased about 0.11% per 10^{-4} Torr pressure, implying nearly a 1% correction to the data taken at about 8×10^{-4} Torr and about a 3% correction to the lower-energy (higher-pressure) data. For the 504.8-nm emission, the pressure dependence was found to be about a factor of four smaller, in agreement with what one calculates using Heddle and Samuel's ideas.[13] For the other emissions, there were no measurable pressure dependences.

The 728.1- and 504.8-nm emission cross sections were corrected for this effect. The HCL uncertainties in the applied corrections were set at $\frac{1}{2}$ the correction magnitude, except at 50 and 100 eV, where the uncertainties were set equal to the correction magnitude because detailed pressure-dependence data were not taken there.

The temperatures T_c and T_R were measured throughout the experiment with calibrated thermocouples at various locations on the cell and reservoir. Normally, T_c was about 35° C and T_R about 24° C. In order to verify the dependence in Eq. (15), T_c was raised with an external heater to 93° C. For the 504.8-nm line at 500 eV, no change within 1% of the measured cross section was observed at the elevated temperatures as long as density was computed using Eq. (15).

B. Electron-beam measurements

The electron gun, collision cell, and electron collector are illustrated in Fig. 4. Also pictured in the cell is a movable Faraday cup–electron-beam-probe assembly which could be lowered through the electron-beam to scan the electron-beam profile $E(y)$ [Eqs. (4) and (5)], and further lowered to measure the electron current entering the cell.

Electrons from the indirectly heated cathode are accelerated and focused onto the aperture pair A_4 and A_5 which determine the size and divergence of the subsequent beam. The beam is then focused onto the center of the collision cell, and finally onto electrode F_5 of the collector assembly. Steering plates at electrodes A_3 and A_6 allow fine adjustment of the beam trajectory through the collision-cell region.

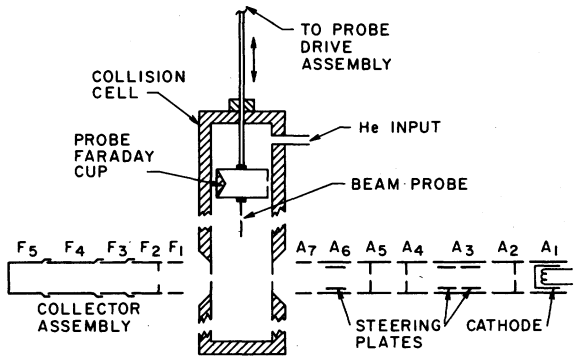

FIG. 4. Schematic of electron gun and collision cell. The probe-Faraday cup can be lowered from outside the vacuum to measure the beam distribution $E(y)$ of Eq. (4), and to measure the total ion current I_e entering the collision chamber.

The beam probe consists simply of an 0.05-mm wide slit through which a portion of the beam could pass. By scanning this probe in the y direction, the shape and extent of $E(y)$ could be mapped on an X-Y recorder. Note that the integral of Eq. (4) is obtained directly, since the probe passes current from all z at a given y. An example of such a scan is shown by the dashed curve in Fig. 5. The base width of $E(y)$ was typically about 0.5 mm, though for 50-eV electrons it was somewhat larger. (The reader will note that this "worst case" situation is shown in Fig. 5.) While not measured, the beam profile was presumably similar in the z direction, since all the electron foc-

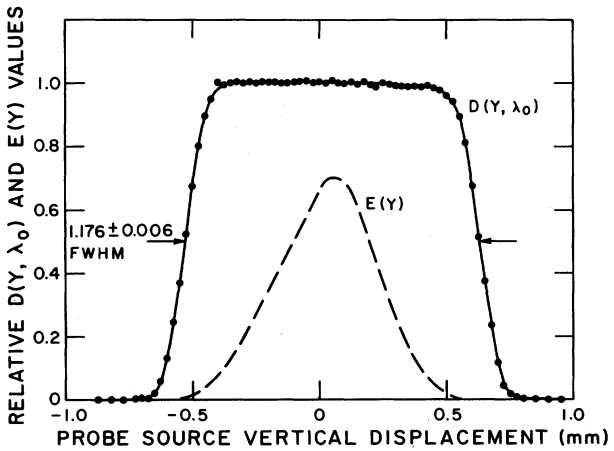

FIG. 5. Dashed curve shows a measured electron-beam distribution $E(y)$ such as appears in Eq. (4). Curve shown is atypical in that it is among the widest of all curves obtained. Points and solid curve represent a measurement of the function $D(y,\lambda_0)$ which is the sensitivity at λ_0 of the spectroradiometer at optical distance z_0 as a function of the vertical coordinate y [see Eqs. (9) and (10)].

using optics had cylindrical symmetry, and the entire apparatus was operated in a Helmholtz coil to eliminate magnetic deflection and distortion of the electron beam.

As shown in Fig. 4, the probe Faraday cup was constructed with a depth to aperture ratio of greater than ten, the cup diameter was large compared to the aperture size, and the surface at the bottom of the cup was inclined relative to the beam so that specularly reflected electrons were driven to the outer walls. On a simple geometric basis, for diffuse reflection, there should be less than 0.2% of the electrons escape from the cup. Since the reflection coefficient should be well below unity, and since there should be some specular character to the reflections, the cup is calculated to be better than 99.8% absorbing. Measurements of currents to A_6 and A_7, movement of the beam within the cup to change the reflections, and comparisons with currents to the final Faraday cup indicated that this assessment of cup absorption is adequate. Thus, the electron current I_e was taken as that entering the collision cell, measured by lowering the very "black" Faraday cup on the probe assembly onto the electron-beam axis. During cross section data runs, the relative electron current was monitored with the efficient collector assembly (F_2 to F_5) beyond the cell. For energies of 500 eV and above, of order 99.8% of the electron beam could be made to completely traverse the cell, but for 100 and 50 eV electrons, this value decreased to about 94% and 90%, respectively, due to beam expansion and scattering in the collision-cell region (~5 cm long).[14] However, even at these low energies, probe measurements determined that all electrons passed within the field of view of the spectroradiometer. These current ratios to the two collectors were accurately determined before and after each cross section measurement run and typically exhibited less than 0.3% change. All currents were measured with instrumentation calibrated daily to better than 0.1%, but the assessed uncertainty of ±0.3% HCL in I_e was increased to ±0.6% at the lower energies to account for this beam divergence problem.

Cross section measurements (at 504.8 nm) were made with a variety of electron-beam profiles $E(y)$ ranging from broad flat ones about 0.8 mm in extent to narrow, peaked ones about 0.3 mm in extent. Within measurement scatter, no dependence of the cross section was apparent so long as $E(y)$ was fully contained in $D(y,\lambda_0)$. (This point will be considered again in Sec. III C, below.) In addition, the cross sections were measured over a range of I_e values and no dependence was observed. Finally, test measurements were made with badly aligned beams such that substantial numbers of electrons were impacting the collision-cell wall in the vicinity of the cell exit aperture. The measured cross section was independent of the fraction of current striking the exit aperture, thus demonstrating the adequacy of the electron current monitoring method. The test also showed that secondary electrons from the (normally) small currents hitting the aperture scatter widely enough that they produce no significant excitation in the viewing region.

C. Spectroradiometer measurements

The overall features of the spectroradiometer have been shown in Fig. 2. Photons were gathered with an apertured achromat lens and focused onto the entrance slit of a Czerny-Turner grating monochromator. Nominally F/7, the system was apertured to give a net speed of F/9.5. This optical system gave rise to about a 1.2 magnification of the electron-beam image at the entrance slit. This image, typically about 0.6 to 1.0 mm tall in the y direction, was always smaller than the actual entrance slit height (~1.5 mm). The entrance slit width (~0.4 mm, giving rise to a wavelength resolution of about 1.0 nm) limited the path length of the electron beam viewed to about 0.32 mm. These dimensions in combination allow the spectroradiometer to accept light from an area of about 0.4 mm^2 on the tungsten strip-lamp filament.

Owing to the small size of the viewing field of the spectroradiometer and the multiplicity of the sources viewed, rather accurate alignment of the instrument was necessary. This was accomplished by passing laser light backwards through the monochromator and observing the emergent light characteristics with a calibrated telescope. It was found possible to locate the optical axis to within a ±0.08-mm transverse uncertainty. Similar studies allowed establishment of the point $z=z_0$ along the axis (the point from which source radiation is "in focus" at the monochromator entrance slit) to within ±0.15-mm uncertainty.

Extensive studies (at several wavelengths) of the spectroradiometer's viewing field in x and y, and its sensitivity to displacements in source position z relative to z_0 were made. Such probing of the viewing field and instrument sensitivity was performed with "point," "thin strip," or extended light sources which were mounted on a micrometer driven support independently movable in any of the x,y,z directions. As an example of the type of data obtained from such studies, a scan over the spectroradiometer's viewing field in the y direction with a thin strip light source (along x) is shown by the solid curve in Fig. 5. This is the function $D(y,\lambda_0)$ of Eq. (10).

Note the rather uniform sensitivity of the spectroradiometer across the top of the scan in the region where $E(y)$ is finite, and the 1.176 ± 0.006-mm full width at half maximum (FWHM) value for the scan. An evaluation of $\mathcal{K}'$ via Eq. (9) for these data gives a value of 1.174 ± 0.006 mm, very close to the FWHM value cited. If the effects of the excited-state lifetimes are included, the $\mathcal{K}$ of Eq. (14) is 1.215 ± 0.008 mm at 416.9 nm, 1.188 ± 0.006 mm at 443.8 nm, and is identical to $\mathcal{K}'$ at 728.1 and 504.8 nm. HCL uncertainties in $\mathcal{K}$ are thus ±0.7% at 416.9 nm and ±0.5% at the other wavelengths.

The dependence of the spectroradiometer's sensitivity to displacements $\pm\Delta z$ about the focus position z_0 was investigated with a thin strip test source (to simulate the electron-beam source) and an extended test source (to simulate the strip-lamp or blackbody sources). As predicted by a simple model for these dependences, the sensitivity was found to be independent of $\pm\Delta z$ for the extended test source and to vary as $z_0/(z_0 \pm \Delta z)$ for the strip source (positive Δz being taken in the direction away from the spectroradiometer's gathering lens). By virtue of the approximation of replacing z by z_0 in the equations in Sec. II, the uncertainty in defining z_0 for the electron-beam and calibration sources, the alignment uncertainty of the electron beam relative to its hypothetical axis, and the uncertainty of the electron-beam diameter in this direction, a HCL uncertainty of ±0.4% is placed on the measured cross sections from this approximation and the establishment of the position z_0.

Size-of-source (SOS) effects were also studied in detail. These effects, which arise from scattering of light as it passes through the various windows and lenses before the monochromator entrance slit, cause the effective area viewed by the spectroradiometer to be slightly increased. For example, for the tungsten strip lamp, one way the SOS_s effect was investigated was by test source simulation of the emitting strip which could be baffled down to successively smaller emitting areas until the actual viewing area of the spectroradiometer was approached, at which point a small extrapolation was made to the actual viewing dimensions. A more effective approach was to use a diffuse reflective screen the size of the strip-lamp filament with variable sized holes at the target area. The SOS_s effect was determined to increase the apparent brightness of this source by $1.0 \pm 0.3\%$. The SOS_e effect for the electron-beam source was found to be less than 0.1%, and the SOS_b effect for the blackbody source was about $1.7 \pm 0.3\%$, large enough so that a slight wavelength dependence could be observed. Appropriate corrections to the light signals measured from these various sources were made and uncertainties included.

While the transmission of the window on the vacuum strip lamp is included in its absolute radiance calibration (to be discussed below), the transmissions of the collision-cell window T_c, and blackbody window T_b, required measurement. Again, these determinations were made with suitable test light sources configured to approximate the actual sources viewed. Transmission data were taken at various wavelengths and agreed well with values predicted for the window material.[15] The uncertainties in the final values adopted were judged to be less than ±0.3% HCL.

The monochromator slit function $S(\lambda - \lambda_0)$, required for evaluation of $\mathcal{L}_s(\lambda_0)$ via Eq. (7), was measured at seven wavelengths between 389 and 728 nm. One such measurement at 504.8 nm, is shown in Fig. 6(a). Note the typical triangular shape of this function and its FWHM value of 0.940 ± 0.003 nm. Even though such measurements proved to be essentially wavelength independent, $\mathcal{L}_s(\lambda_0)$ values were always computed using two such functions at or nearby the wavelengths of interest. The maximum difference encountered between such pairs of data was ±0.4% and it was thus judged that ±0.6% should represent a HCL uncertainty in $\mathcal{L}_s(\lambda_0)$ from this source.

Figure 6(b) shows $S(\lambda - \lambda_0)$ over expanded transmission and wavelength ranges (solid curve). Note that $S(\lambda - \lambda_0)$ drops rapidly to about 2×10^{-3} of its value at λ_0, but persists at a finite value (10^{-3} to 10^{-5}) out to large $\lambda - \lambda_0$. Thus, if the monochromator were the only dispersive element in the spectroradiometer, when viewing a continuum source such as the strip lamp, there would be large contributions to the observed signal from wavelengths very distant from λ_0. This problem was particularly severe at the shorter wavelengths of interest here, because $L_s(\lambda)$ is such a rapidly increasing function of λ.

This was, of course, the reason why interference filters were used to enhance the wavelength discrimination properties of the spectroradiometer. The normalized filter transmission curve $F(\lambda)$ is shown by the long-dashed curve in Fig. 6(b) and the product $S(\lambda - \lambda_0)F(\lambda)$ by the lower short-dashed curve. Even here, however, a potential problem exists at the 416.9-nm He line. Our best estimates suggest that $\mathcal{L}_s(\lambda_0)$ contains an 0.05% contribution from the $600 < \lambda < 800$ nm region, where $L_s(\lambda)$ is 10^3 to 10^4 times brighter than at 416.9 nm. Because neither $S(\lambda - \lambda_0)$ nor $F(\lambda)$ were determined accurately this far from λ_0 at this wavelength, an additional HCL uncertainty of ±0.5% (i.e., 10 times our estimate) has been placed on $\mathcal{L}_s(\lambda_0)$ from this source. At the other

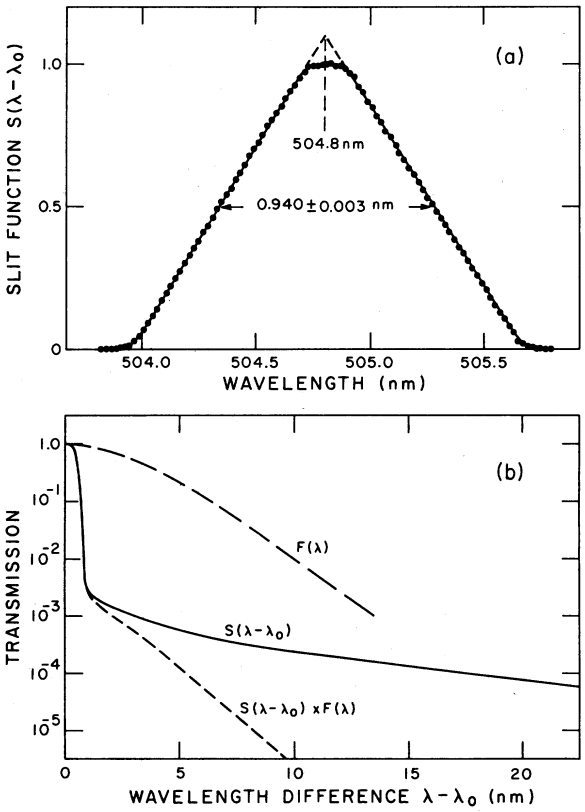

FIG. 6. (a) Monochromator slit function $S(\lambda-\lambda_0)$ as measured with $\lambda_0=504.8$ nm. (b) Solid curve is monochromator slit function $S(\lambda-\lambda_0)$ with logarithmic ordinate. $F(\lambda)$, shown by the long-dashed curve, is the normalized interference filter transmission. The product function giving the net transmission of the spectroradiometer as used in Eq. (7) is shown by the short-dashed curve.

wavelengths of interest, this effect should be negligible ($\ll 0.1\%$).

The broad bandpass interference filters used had typical FWHM values of 10 nm. After consideration of their wavelength transmission profiles $F(\lambda)$, which remained near unity for $|\lambda-\lambda_0| \lesssim 1$ nm, and the changes in these profiles with photon angle of incidence and temperature, a HCL uncertainty ±0.4% was assigned to use of the approximation of Eq. (6).

At the very heart of this experiment are the problems of doing absolute radiometry and accurately assessing the uncertainties encountered. The tungsten strip lamp employed as a day-to-day radiance standard was calibrated to better than 0.8% at selected wavelengths (455.4, 493.4, 654.6 nm) by the Optical Radiation Section of the National Bureau of Standards (NBS) against the gold-point blackbody radiance standard. Radiances at other wavelengths had to be inferred using emissivity data and the NBS assessment of the uncertainty associated with use in this fashion, when their carefully specified operating conditions are followed, is ±2.0%. $L_s(\lambda)$ is assigned this uncertainty.

A combination of this value in quadrature with the uncertainties cited here for determination of $S(\lambda-\lambda_0)$, use of $F(\lambda)$, and the SOS_s effect, leads to a net uncertainty ±2.1% in $\mathcal{L}_s(\lambda_0)$, except at 416.9 nm where the problem of the contribution from the filtered slit function wing regions increases the value to ±2.2%. Note, however, that the 2% NBS figure for $L_s(\lambda)$ includes an uncertainty in the extrapolation to other wavelengths using published emissivities. There is no clear way to relate this 2% uncertainty to what we are calling HCL in this paper.

Because of the large magnitude of these uncertainties and our earlier stated philosophy of attempting to measure all experimental variables by more than one procedure, a copper-point blackbody radiance standard was constructed. Such melting-point blackbodies are ideal standards since the radiance $L_b(\lambda)$ and uncertainty are, at least in principle, determined by the melting point of the element used. The construction and operation of the blackbody employed here are described in the Appendix. The computation of $\mathcal{L}_b(\lambda_0)$ proceeds in a way similar to the use of Eq. (7) for computing $\mathcal{L}_s(\lambda_0)$. Our assessment of the HCL uncertainties in $\mathcal{L}_b(\lambda_0)$ yields ±1.2% (1.3% at 416.9 nm).

Since the observed photon count rates R_s and R_b should be in direct proportion to $\mathcal{L}_s(\lambda_0)$ and $\mathcal{L}_b(\lambda_0)$, it was possible to "predict" a value for the reduced strip-lamp radiance from the relationship

$$\mathcal{L}_s^p(\lambda_0)=\mathcal{L}_b(\lambda_0)\left(\frac{R_s}{R_b}\right)\left(\frac{SOS_B}{SOS_S}\right), \tag{16}$$

by using $\mathcal{L}_b(\lambda_0)$ as a local standard. The procedures used for such comparisons between the strip-lamp and blackbody radiances are discussed in the Appendix. The results yield $\mathcal{L}_s^p(\lambda_0)$ values averaging 1.9% below those for $\mathcal{L}_s(\lambda_0)$, being lower by 2.2%, 1.8%, 2.1%, and 1.5% at 416.9, 443.8, 504.8, and 728.1 nm, respectively.

It was reassuring to find that $\mathcal{L}_s^p(\lambda_0)$ and $\mathcal{L}_s(\lambda_0)$ were within mutual uncertainties, but bothersome, nevertheless, that the difference was so large and clearly systematic in character, as can be seen from its essential wavelength independence. There are a number of difficulties associated with properly using a strip lamp. For example, a large radiance gradient with vertical position on the strip-lamp filament (~6% per mm) could cause serious error if either the NBS or local determinations of the position viewed were incorrect.

While such arguments would tend to support use of our blackbody as a radiance standard for this experiment, the existence of a perplexing problem found in employing this standard at wavelengths short of 400 nm causes us to temper this judgment (see the Appendix for a discussion of the difficulty). After due consideration, we adopted a value half-way between $\mathcal{L}_s^p(\lambda_0)$ and $\mathcal{L}_s(\lambda_0)$ as the reduced radiance standard for this experiment. The uncertainty claimed is ±2.1%, a value liberally encompassing both $\mathcal{L}_s^p(\lambda)$ and $\mathcal{L}_s(\lambda_0)$, including all the range of uncertainty cited for $\mathcal{L}_s^p(\lambda_0)$, taken here as that ascribed to $\mathcal{L}_b(\lambda_0)$, and over $\frac{3}{4}$ of that cited for $\mathcal{L}_s(\lambda_0)$. In our judgment, this uncertainty represents a true HCL value.

A typical cross section measurement proceeded as follows. After alignment of the electron beam and measurement of its profile $E(y)$, the electron current and pressure measurement instruments were calibrated. The spectroradiometer was rotated to view the strip lamp for its radiometric calibration. Signals from e-He collisions were then measured, after which the calibrations were again performed. An average "calibration factor" [the square-bracketed parameters in Eq. (8)] was used to reduce the data. The maximum difference ever found for such factors determined from the calibration data before and after the signal measurement was ±0.6%, a value taken as a HCL uncertainty in assessing instrumentation sensitivity drifts over a cross section measurement period. Count rate, pressure, and electron current were accumulated for preset times (along with other housekeeping information) and digitized for analysis. The line-emission cross sections were computed for each measurement time for statistical evaluation at the 98% CL level, and subsequently combined in quadrature with the net calibration factor uncertainty to yield the net HCL uncertainty cited in the next section.

IV. RESULTS AND DISCUSSION

The line-emission cross sections determined from measured quantities used in Eq. (8) with defining Eqs. (4), (7), (10), and (14) are listed in Table I. The HCL uncertainties are a combination of counting statistical uncertainties and systematic uncertainties combined as discussed at the end of Sec. II. Individual sources of systematic uncertainty are summarized in Table II.

These line-emission cross sections should be usable by those wishing to calibrate excitation apparatus after they have corrected for pressure dependences in their systems. As seen, the most accurate results are for 500-eV energy, where the mean uncertainty is only 3.5% HCL, compared to mean uncertainties of 9, 7, 6, and 5% HCL at 50, 100, 1000, and 2000 eV, respectively.

It is, of course, interesting and valuable to compare the results here with theory and with other measurements. Theoretical calculations are normally of level-excitation cross sections, so we must either construct line-emission cross sections from the proper assortment of level-excitation cross sections or derive level-excitation cross sections from the measured line-emission cross sections. We choose the latter course, since that is what has been done in most of the past experiments and the original data are, in some instances, not even available for the line-emission cross sections.

In our experiment, the $n\,^1S$ levels are populated by collisions directly to the level, by collisions

TABLE I. Helium line-emission cross sections.[a]

Electron energy (eV)	Line-emission cross sections σ_{ns}^0 (10^{-20} cm^2) 728 (nm) ($3\,^1S \rightarrow 2\,^1P$)	505 (nm) ($4\,^1S \rightarrow 2\,^1P$)	444 (nm) ($5\,^1S \rightarrow 2\,^1P$)	417 (nm) ($6\,^1S \rightarrow 2\,^1P$)
50	35.2 ± 2.9	8.08 ± 0.58	3.09 ± 0.27	1.46 ± 0.16
100	24.9 ± 2.8	5.61 ± 0.25	2.30 ± 0.12[b]	0.97 ± 0.07[c]
500	9.23 ± 0.32	2.05 ± 0.057	0.78 ± 0.026	0.374 ± 0.016
1000	5.11 ± 0.32	1.11 ± 0.036	0.425 ± 0.022	0.212 ± 0.019
2000	2.75 ± 0.15[d]	0.583 ± 0.024	0.223 ± 0.010	0.108 ± 0.006

[a] From measured quantities used in Eq. (8), corrected to zero density. Uncertainties are high confidence level uncertainties (HCL), roughly equivalent to 98% (CL) and are a quadrature combination of statistical and systematic uncertainties shown in Table II.

[b] Analysis of a series of systematic trends of the data indicates that this number should probably be about 2.14, a number somewhat outside the quoted uncertainty.

[c] Analysis of a series of systematic trends of the data indicates that this number should probably be about 1.01, a number well within the quoted uncertainty.

[d] Analysis of a series of systematic trends of the data indicates that this number should probably be about 2.67, a number well within the quoted uncertainty.

TABLE II. Summary of HCL uncertainties as discussed in Sec. III.[a]

Uncertainty source	Uncertainty (%)
I_e, electron current[b]	0.3
N_{He}, helium density[c]	1.2
$\mathcal{L}(\lambda_0)$, reduced radiance of standard as per Eq. (7)[d]	2.1
$\mathcal{H}$, effective height as per Eq. (14)[e]	0.5
z_0, distance of source to spectroradiometer target	0.4
Calibration drifts during measurements	0.6
Size of source effect	0.1
T_c, transmission collision-cell window	0.3
Pressure dependence of cross section[f]	0–3

[a] Quantities are those in Eq. (8) and defining Eqs. (4), (7), (10), and (14).
[b] For 50 and 100 eV, the uncertainty is 0.6%.
[c] For 50 and 100 eV, the uncertainty is 3%.
[d] For 417 nm, the uncertainty is 2.2%.
[e] For 417 nm, the uncertainty is 0.7%.
[f] For 417 and 444 nm the correction and uncertainty are zero. For 728 nm the uncertainty is 3% at 50 and 100 eV and 0.2% at higher energies. For 505 the uncertainty is 0.7% at 50 and 100 eV and 0.1% at higher energies.

to higher-P states which cascade into $n\,^1S$, and by collisions to higher-S and -D states which cascade into higher-P states and in turn to $n\,^1S$. We ignore the latter "multiple cascade" sources and write the level population cross section:

$$\sigma_i^p = \sigma_i^e + \sum_{j>i} \sigma_j^e A_{ji} \tau_j$$

$$= \sigma_i^e + \sum_{j>i} \sigma_j^e \gamma_{ji} ,$$

where the A_{ji} are the Einstein A coefficients between higher-P levels and the relevant $n\,^1S$ level denoted by i, and τ_j is the lifetime of level j. The γ_{ji} are branching ratios. The line-emission cross sections which we observed and which are tabulated in Table I are

$$\sigma_i^0 = \sigma_i^p A_{i1} \tau_i = \sigma_i^p \gamma_{i1} ,$$

where A_{i1} is the Einstein A value between $n\,^1S$ and the lower $2\,^1P$ level.

Then we have for the level-excitation cross section

$$\sigma_i^e = \sigma_i^0/\gamma_{i1} - \sum_{j>i} \sigma_j^e \gamma_{ji} . \qquad (17)$$

To determine the σ_i^e from Eq. (17), we have used the σ_{np}^e values of Moustaffa Moussa *et al.*[16] for $n = 3, 4, 5$. For higher n, we have taken[17,18] as an approximation $\sigma_{np}^e = (5/n)^3 \sigma_{5p}^e$. Branching ratios have been calculated from A values tabulated by Wiese *et al.*[8] for $n \leq 8$, and have been set equal to a constant 8×10^{-3}, 4×10^{-3}, 1.5×10^{-3}, and 1.5×10^{-3} for branching from higher-P states ($n>8$) to the $3\,^1S$, $4\,^1S$, $5\,^1S$, and $6\,^1S$ levels, respectively. Table III lists the σ_{ns}^e obtained from this evaluation.

TABLE III. Level-excitation cross sections obtained using Eq. (17) and the line-emission cross sections of Table I.

Electron energy (eV)	Level-excitation cross sections σ_{ns}^e (10^{-20} cm^2) $3\,^1S$	$4\,^1S$	$5\,^1S$	$6\,^1S$
50	33.7	13.3	6.42	3.40
100	23.3	9.06	4.74	2.23
500	8.45	3.26	1.58	0.849
1000	4.63	1.76	0.862	0.479
2000	2.45	0.906	0.447	0.241

Comparisons of these cross sections with other work, both experimental and theoretical, are shown in Fig. 7, where the ratio of other cross sections to the present ones are plotted versus the logarithim of electron energy in eV. The solid curves are the Born-approximation results of Inokuti and Kim.[17,18] (The results of Kingston *et al.*[19] match those of Inokuti and Kim within a few tenths percent at 2 keV, and are generally about 4% smaller at 50 eV.) It is seen that by 2 keV, the Born approximation describes the cross sections quite accurately, the deviations being 0, 2.6, 1.8, and 5.6% for $n = 3$, 4, 5, and 6, respectively. Similarly, the results of Scott and McDowell[20,21] using the distorted-wave polarized-orbital approximation (DWPO), shown by open circles connected by a dotted curve, seem to predict within 10% the cross sections at 50 and 100 eV, where the Born approximation gives values too high by about a factor of two.

Measurements shown in the figures include those of Moustaffa Moussa *et al.*[16] (+'s connected by short dashes) which differ from the present measurements an average of only 6%; St. John *et al.*[22] (*s*'s connected by solid line) which differ from the present measurements an average of 32%; Aarts *et al.*[23] (open squares connected by long dashes) which differ by an average of 14%; Van Raan *et al.*[24] (open triangles connected by dash-dots) which differ by an average of 18%; Showalter and Kay[25] (solid squares connected by dots) which differ by an average of 15%; McConkey and Woolsey[26] (solid circles connected with dash-double dot) which differ an average of 39%; Gabriel and Heddle[27] (G's) which differ by an average of 70%; and Lees[28] (L's connected with dashes) which differ by an average of 15%. It is not possible to

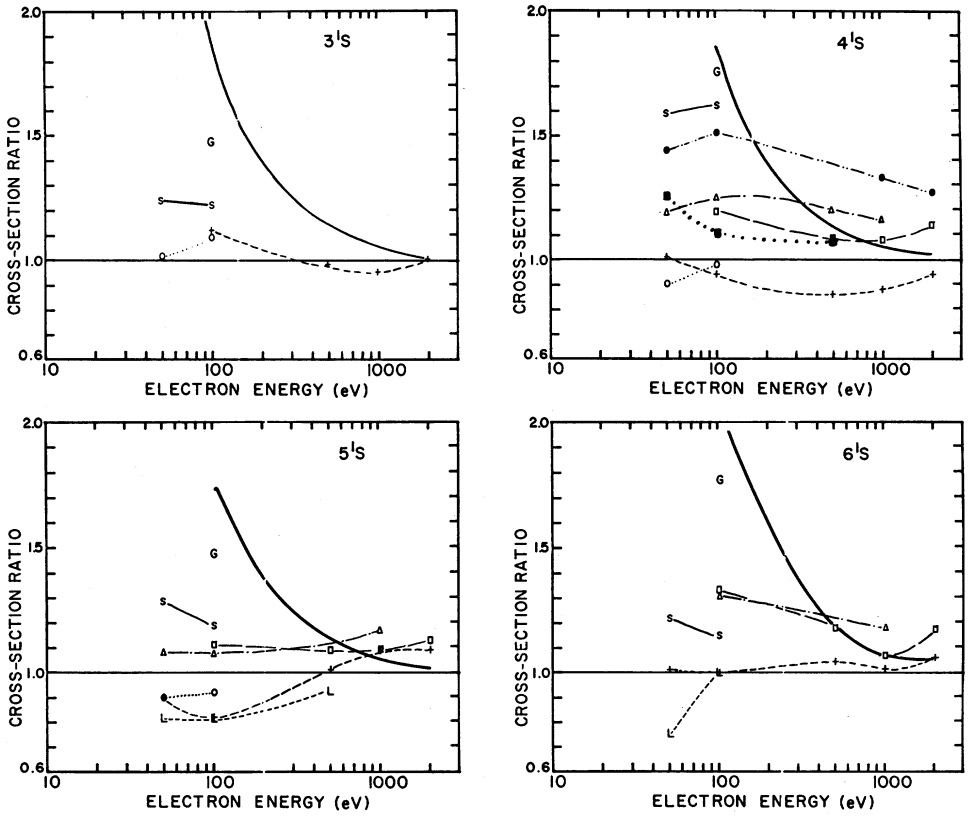

FIG. 7. Ratio of cross sections measured and calculated by others to the present measurements. For level-excitation cross sections: Solid curve, approximation (Refs. 17 and 18); ○, distorted-wave polarized-orbital (Refs. 20 and 21); +, Moustaffa Moussa *et al.* (Ref. 16); *s*, St. John *et al.* (Ref. 22); □, Aarts *et al.* (Ref. 23); △, Van Raan *et al.* (Ref. 24); ●, McConkey and Woolsey (Ref. 26); G, Gabriel and Heddle (Ref. 27). For line-emission cross sections: ■, Showalter and Kay (Ref. 25); L, Lees (Ref. 28).

show the results of all other workers[1-4] in Fig. 7. Other results often compared in the literature are those of Yakhontova,[29] Zapesochnyi *et al.*,[30] and Thieme.[31] These latter results are all consistently higher than the present ones by up to more than a factor of two.

From these figures, we again emphasize: (1) The good agreement between the present results and the Born approximation at the highest energy (2 keV), (2) the good agreement between the present results and the results of Moustaffa Moussa *et al.*,[16] and (3) the reasonable agreement with the DWPO of Scott and McDowell[20,21] at lower energies. It is further a remarkable fact that the 1932 results of Lees,[28] where observation and measurement of light was done photographically, are essentially the next closest results (the 15% average deviation being essentially the same as Aarts *et al.*).[23]

ACKNOWLEDGMENTS

Support from the National Standard Reference Data System is gratefully acknowledged.

APPENDIX: THE COPPER-POINT BLACKBODY

The construction of the copper-melting-point blackbody used as a radiance standard in this work is shown in Fig. 8. The thin-walled radiation cavity was machined from high-purity graphite and surrounded by the copper sample[32] to be melted. This assembly was immersed in an additional graphite environment and spring loaded with stainless steel spacers at each end into a ceramic tube about which the heating coils were wound. Multilayers of loosely rolled ceramic paper served to insulate this heated tube from the stainless steel vacuum wall. A 2-mm-thick quartz window provided the vacuum seal at the output end of the system.

The construction materials and their dimensions were chosen to keep the heat capacity per unit length as constant as possible. The heater winding was divided into three independently controlled sections, and the powers required for each section were computed from an analysis of the radiative and conductive heat losses from the various

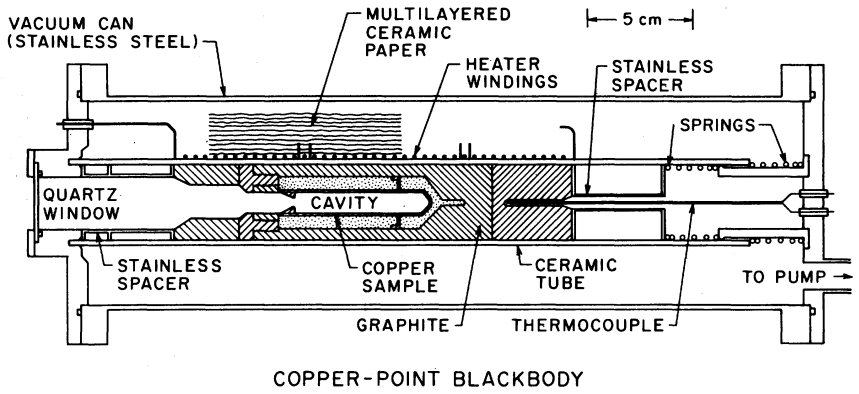

FIG. 8. Schematic view of the copper-point blackbody.

interior component surfaces. The achievement of these balanced power requirements was found to be essential to proper operation. At operating temperature, the total power required was about 500 W.

The operation of the blackbody typically proceeded as follows. The unit was evacuated and back filled to about 20 Torr of argon (at room temperature). Heater power was applied and the temperature increase monitored with the thermocouple until about 1300 K was reached. At this point, the spectroradiometer was rotated into position to accept radiation from the cavity. The time sequence of events is now picked up in Fig. 9. As can be seen, the observed spectroradiometer count rate increased rapidly until the melting temperature of the copper sample was reached, at which point the count rate reached a plateau. At this time, the heating power was being used to effect the solid-liquid phase change of the sample, at a constant temperature of 1358.0 K. After all the sample had been melted, the temperature (and thus the observed count rate) again began to increase.

After decreasing the input power, and allowing for a temperature overshoot, the count rate began to decrease until the sample temperature again reached 1358 K. After a supercooling minimum, the temperature again remained at this level until the entire sample had been solidified. The melt-freeze cycle was now completed, but could be repeated if desired.

The time intervals for which no data points are shown were used to observe radiation at other wavelengths or to observe radiation from the tungsten strip lamp. Thus, rather good comparisons between the blackbody and strip-lamp sources could be made. Such radiance comparison data were obtained from seven different melt-freeze cycles over a period of three days. The standard deviation of the mean of the radiance ratios from these sources was 0.2% at 728.1 nm and less than 0.1% at the other wavelengths of interest.

As mentioned in Sec. III of this paper, it was possible to predict the radiance of the strip-lamp source by using the blackbody as a standard [via Eq. (2)]. These predictions led to the conclusion that the calibrated strip-lamp radiance was high or the blackbody radiance low, by 1.9%, a value which was found to be essentially wavelength independent. Other work in this laboratory required absolute radiance standards at wavelengths short of 400 nm. In this region, the apparent radiance of the blackbody increased relative to the strip lamp and was found to be about 10% higher than the strip lamp in the 300-nm region. In fact, with earlier versions[33] of the blackbody which were operated at atmospheric pressure, it was found their apparent radiances were more than a factor of two above those of the strip lamp near 300 nm, even though the two sources agreed well in the wavelength region above 400 nm. For this reason the "evacuated" blackbody was constructed.[34] While the wavelength and pressure dependence of this problem were thus roughly characterized, the cause of this difficulty has not been positively

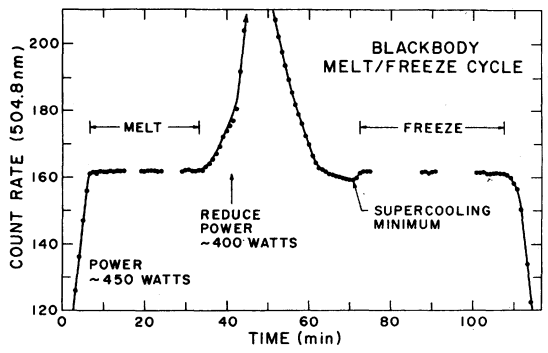

FIG. 9. Typical melt-freeze cycle of the blackbody. Open periods in the sequence of points occur at times when the spectroradiometer was tuned to another wavelength or moved to view the vacuum strip lamp.

identified at this time.

It had been our plan to use the blackbody as the radiance standard for this work, because its radiance uncertainty was found to be smaller than that for the strip lamp. However, even though there is no evidence of any sort to suggest that this problem exists at wavelengths above 400 nm, and considerable evidence to suggest that it does not, the unresolved nature of this perplexing difficulty caused us to reconsider this plan. Note that if a small remnant of this problem persisted at the longer wavelengths, it would cause the $\mathcal{L}_s^p(\lambda_0)$ values to be too high, increasing the disparity between our blackbody and the NBS calibrated strip-lamp radiances. As discussed in Sec. III, a value for the calibration source radiance half-way between those found for the blackbody and calibrated strip-lamp sources was finally adopted, with an uncertainty sufficient to encompass both determinations.

---

*Present address: University of Denver, Denver, Colo.
†U. S. National Bureau of Standards, Boulder, Colo. 80302.
‡Present address: Physics Department, Royal Holloway College, Egham, Surrey, England.

[1]L. J. Kieffer, Natl. Bur. Stand. (U. S.) Spec. Publ. 426, 25 (1976); 426, 28 (1976).
[2]J. W. Gallagher, J. W. Rumble, Jr., and E. C. Beaty, Natl. Bur. Stand. (U.S.) Spec. Publ. 426, 13 Suppl. 1 (1979); 426, 14 Suppl. 1 (1979).
[3]J. W. Gallagher and E. C. Beaty, JILA Information Center Report No. 18, 1980 (unpublished).
[4]L. J. Kieffer, At. Data 1, 120 (1969).
[5]B. L. Moiseiwitsch and S. J. Smith, Rev. Mod. Phys. 40, 238 (1968).
[6]D. W. O. Heddle and R. G. W. Keesing, in *Advances in Atomic and Molecular Physics*, edited by D. R. Bates and I. Estermann (Academic, New York, 1968), p. 267.
[7]H. S. W. Massey and E. M. S. Burhop, *Electronic and Ionic Impact Phenomena* (Oxford University Press, London, 1969), Vol. 1, p. 169.
[8]W. L. Wiese, M. W. Smith, and B. M. Glennon, *Atomic Transition Probabilities* (National Standard Reference Data Series, National Bureau of Standards, Washington, D.C., 1966), Vol. I.
[9]H. R. Moustafa Moussa, Ph. D. thesis, University of Leiden, 1967 (unpublished).
[10]A. F. J. Van Raan, J. P. De Jongh, J. Van Eck, and H. G. M. Heideman, Physica (Utrecht) 53, 45 (1971).
[11]B. Van Zyl, G. E. Chamberlain, and G. H. Dunn, J. Vac. Sci. Technol. 13, 721 (1976).
[12]Reference 11 discusses our measurements using this "direct" method and a rough uncertainty of ±2% was presented there. The larger figure of ±3% is taken here to represent HCL.
[13]D. W. O. Heddle and M. J. Samuel, J. Phys. B 3, 1593 (1970).
[14]To minimize the collection "problem" and other difficulties which could be caused by excessive space charge, electron currents were kept to approximately 2, 6, 70, 115, and 200 μA at 50, 100, 500, 1000, and 2000 eV electron energy, respectively. This slight divergence does not affect the assumption of a beam traveling parallel to the x axis which went into writing Eq. (4). The beam divergence is only of order 2° or less, and over the 0.3-mm section of beam along x which the monochromator "sees," the y extent of the beam changes less than 2%. The detectivity of the optical system is constant over this small change, and no error is introduced. The path length through the target of the most extreme electron is increased by less than 0.1%.
[15]I. H. Malitson, J. Opt. Soc. Am. 55, 1205 (1965).
[16]H. R. Moustaffa Moussa, F. J. DeHeer, and J. Schutten, Physica (Utrecht) 40, 517 (1969).
[17]M. Inokuti and Y.-K. Kim, Phys. Rev. 186, 100 (1969).
[18]Y.-K. Kim and M. Inokuti, Phys. Rev. A 3, 665 (1971).
[19]K. L. Bell, D. J. Kennedy, and A. E. Kingston, J. Phys. B 2, 26 (1969).
[20]T. Scott and M. R. C. McDowell, J. Phys. B 8, 1851 (1975).
[21]T. Scott and M. R. C. McDowell, J. Phys. B 8, 2342 (1975).
[22]R. M. St. John, F. L. Miller, and C. C. Lin, Phys. Rev. 134A, 888 (1964).
[23]J. F. M. Aarts, F. J. DeHeer, and D. A. Vroom, Physica (Utrecht) 40, 197 (1968).
[24]A. F. J. Van Raan, J. P. DeJongh, J. Van Eck, and H. G. M. Heideman, Physica (Utrecht) 53, 45 (1971).
[25]J. G. Showalter and R. B. Kay, Phys. Rev. A 11, 1899 (1975).
[26]J. W. McConkey and J. M. Woolsey, in *Abstracts of Papers, VI International Conference on the Physics of Electronic and Atomic Collisions*, edited by I. Amdur (MIT Press, Cambridge, Mass., 1969), p. 355.
[27]A. H. Gabriel and D. W. O. Heddle, Proc. R. Soc. London Ser. A 258, 124 (1960).
[28]J. H. Lees, Proc. R. Soc. London Ser. A 137, 173 (1932); 137, 186(E) (1932).
[29]V. E. Yakhontova, Vestn. Leningr. Univ. Ser. Mat. Fiz. Khim. 14, 27 (1959). (Translation: 951 by Atomic Energy Research Establishment, Harwell, Berkshire, England.)
[30]I. P. Zapesochnyi and P. V. Feltsan, Ukr. Fiz. Zh. 10, 1197 (1965).
[31]O. Thieme, Z. Phys. 78, 412 (1932).
[32]NBS-certified freezing-point standard reference material—lot 45d. Freezing temperature of sample = 1358.0 ± 0.5 K.
[33]Earlier versions were constructed according to R. D. Lee, *Construction and Operation of a Simple High-Precision Copper-Point Blackbody and Furnace*, Natl. Bur. Stand. Tech. Note No. 483 (U. S. GPO, Washington, DC, 1969).
[34]An attempt to operate the blackbody in a totally evacuated mode led to deposition of copper on the quartz window.
[35]J. D. Jobe and R. M. St. John, Phys. Rev. 164, 117 (1967).
[36]F. L. Miller, Ph. D. thesis, University of Oklahoma, 1964, University Microfilms, Inc., Ann Arbor, Michigan No. 64-11, 760 (unpublished).